Advances in Rock-Support *and* Geotechnical Engineering

Shuren Wang, Paul C. Hagan, and Chen Cao

ADVANCES IN ROCK-SUPPORT AND GEOTECHNICAL ENGINEERING

SHUREN WANG
PAUL C. HAGAN
CHEN CAO

AMSTERDAM • BOSTON • HEIDELBERG • LONDON
NEW YORK • OXFORD • PARIS • SAN DIEGO
SAN FRANCISCO • SINGAPORE • SYDNEY • TOKYO
Butterworth-Heinemann is an imprint of Elsevier

Butterworth-Heinemann is an imprint of Elsevier
The Boulevard, Langford Lane, Kidlington, Oxford OX5 1GB, United Kingdom
50 Hampshire Street, 5th Floor, Cambridge, MA 02139, United States

Notices
Knowledge and best practice in this field are constantly changing. As new research and experience broaden our understanding, changes in research methods, professional practices, or medical treatment may become necessary.

Practitioners and researchers must always rely on their own experience and knowledge in evaluating and using any information, methods, compounds, or experiments described herein. In using such information or methods they should be mindful of their own safety and the safety of others, including parties for whom they have a professional responsibility.

To the fullest extent of the law, neither the Publisher nor the authors, contributors, or editors, assume any liability for any injury and/or damage to persons or property as a matter of products liability, negligence or otherwise, or from any use or operation of any methods, products, instructions, or ideas contained in the material herein.

Library of Congress Cataloging-in-Publication Data
A catalog record for this book is available from the Library of Congress

British Library Cataloguing in Publication Data
A catalogue record for this book is available from the British Library

ISBN: 978-0-12-810552-8

Publisher: Jonathan Simpson
Acquisition Editor: Simon Tian
Editorial Project Manager: Vivi Li
Production Project Manager: Susan Li
Designer: Maria Inês Cruz

Typeset by TNQ Books and Journals

Biography

Shuren Wang, PhD, Professor at School of Civil Engineering, Henan Polytechnic University, Jiaozuo 454003, China. Contact details: +86 15738529570; w_sr88@163.com.

His research interests primarily includes the challenging areas of mining engineering, geotechnical engineering, rock mechanics, and numerical simulation analysis. His research projects have been supported by National Natural Science Foundation of China (51474188; 51074140; 51310105020), National Natural Science Foundation of Hebei Province of China (E2014203012), Science and Technology Department of Hebei Province of China (072756183), and so forth. He is the recipient of six state-level and province-level awards and the 2015 Endeavor Research Fellowship provided by the Australian Government. He has authored more than 90 academic papers and books. These include 85 articles in peer-reviewed journals, six monographs, and numerous textbooks. He has been authorized four patents and one software of intellectual property right in China.

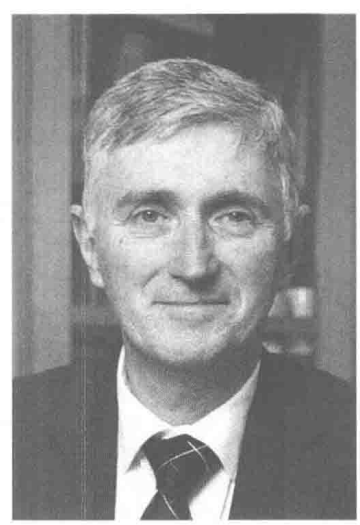

Paul C. Hagan, PhD, Associate Professor, Head of School of Mining Engineering, University of New South Wales (UNSW), Sydney, NSW 2052, Australia. Contact details: +61 2 9385 5998; p.hagan@unsw.edu.au.

His principal research interests include mine geotechnical engineering and other areas in mining engineering. He has more than 30 years of experience within the mining industry and university sectors. Prior to his appointment to UNSW in 1998, he worked locally and

internationally in the coal, gold, and iron ore sectors in a range of operational, management, technical, and research roles. He has been the principal research investigator of leading projects in the rock-cutting research facility. The research has made significant advances in the application of acoustic emissions in monitoring and control of rock-cutting machines and in the determination of controlling factors associated with abrasivity testing of rock. He has authored 80 peer-reviewed papers, 110 project reports, and three patents.

Chen Cao, PhD, Research Fellow at School of Civil, Mining, and Environmental Engineering, University of Wollongong, NSW 2530, Australia. Contact details: +61 2 4221 7945; ccao@uow.edu.au.

After he graduated from Xi'an Jiaotong University, China with a bachelor's degree in science, he worked in computer engineering and had nine years of experience in the field of construction and management. He obtained a Bachelor of Engineering degree in 2009 and received a PhD degree with distinguished award for his PhD thesis from the University of Wollongong in 2013. He has been mainly involved in rock mechanics, mining engineering, and numerical simulation, and has made many breakthroughs at dealing with the problems with complex geological and engineering conditions, especially in large shear displacement by mining pressure and other factors on rock bolting and anchor support. He has authored more than 20 academic papers in the research field.

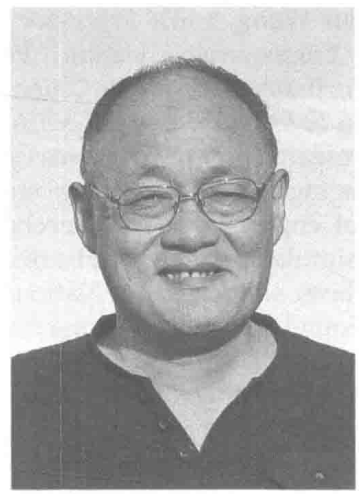

Preface

There have been significant advances in rock mechanics and understanding of the behavior of rock with developments in science and engineering. This has occurred at the same time as there has been greater demand for the utilization of underground space that has in many cases pushed the limits in the engineering design of underground excavations while there has been the continual need to improve safety and reduce the cost of excavation. It is imperative, then, that research continues which will provide the knowledge necessary to underpin the design and development of new excavation techniques.

The book summarizes and enriches the latest research results on the theory of rock mechanics, analytical methods, innovative technologies, and its applications in practical engineering. The book is divided into six chapters including such features as Chapter 1: Rock Testing (Shuren Wang Sections 1–7; Paul Hagan Section 8); Chapter 2: Rock Bolting (Chen Cao Sections 1–7; Paul Hagan Section 8); Chapter 3: Grouted Anchor (Paul Hagan); Chapter 4: Tunneling Engineering (Shuren Wang); Chapter 5: Slope Engineering (Shuren Wang); and Chapter 6: Mining Geomechanics (Shuren Wang). This book is innovative, practical, and rich in content, which can be of great use and interest to the researchers undertaking various geotechnical engineering and rock mechanics, teachers and students in the related universities, as well as on-site technicians.

The material presented in this book contributes to the expansion of knowledge related to rock mechanics. The authors, through their extensive fundamental and applied research over the past decade, cover a diverse range of topics from the microbehavior of rock and rock properties through the interaction of large-scale rock masses and its effect on surface subsidence, mechanics of rock cutting, techniques to improve the strength and integrity of rock structures in surface and underground excavations, and improvement in approaches to modeling techniques used in engineering design.

Shuren Wang, PhD
Professor at School of Civil Engineering, Henan Polytechnic University, China
Paul C. Hagan, PhD
Associate Professor and Head of School of Mining Engineering, University of New South Wales, Australia
Chen Cao, PhD
Research Fellow at School of Civil, Mining and Environmental Engineering, University of Wollongong, Australia

Acknowledgments

The authors are pleased to acknowledge the support received from various organizations, including the National Natural Science Foundation of China (51474188; 51074140; 51310105020); the Natural Science Foundation of Hebei Province of China (E2014203012); the China Scholarship Council (CSC); the Hebei Provincial Office of Education (2010813124); 2015 Endeavor Research Fellowship and Program for Taihang Scholars; International Cooperation Project of Henan Science and Technology Department (162102410027); Doctoral Fund of Henan Polytechnic University (B2015-67); Opening Project of Key Laboratory of Deep Mine Construction; Provincial Key Disciplines of Civil Engineering of Henan Polytechnic University; and the School of Mining Engineering, University of New South Wales.

While it is not possible to name them all, the authors are particularly thankful to Prof. Manchao He, Prof. Meifeng Cai, Prof. Ji'an Wang, Prof. Youfeng Zou, Prof. Xiaolin Yang, Prof. Xiliang Liu, Prof. Zhaowei Liu, Prof. Zhengsheng Zou, Prof. Jianhui Yang, Prof. Yanbo Zhang, and other related people. A number of postgraduate students, namely Jianhang Chen, Li Li, Chunliu Li, Haiqing Zhang, Yan Cheng, Baowen Hu, Chengguo Zhang, Peipei Liu, Huihui Jia, Hu Wang, Mengshi Chang, Zhongqiu Wang, Ning Li, Dianfu Xu, Yongguang Wang, Junqing Su, Huaiguang Xiao, Yanhai Zhao, Chunyang Li, and others assisted in the design, construction, and commissioning of the test facility and with the experimentation; their contributions to the book are acknowledged and appreciated. The untiring efforts of Mr. Kanchana Gamage, Dr. Juninchi Kodama, Dr. Mojtaba Bahaaddini, and Dr. Hossein Masoumi during equipment design and laboratory testing programs are gratefully appreciated. Thanks and apologies to others whose contributions we have overlooked.

Contents

6. Mining Geomechanics

CHAPTER

1

Rock Testing

1. INSTABILITY CHARACTERISTICS OF A SINGLE SANDSTONE PLATE

1.1 Introduction

In China, numerous shallow mined-out areas have been left due to the disordered mining by the private coal mines. It is of important theoretical and practical value for the roof stability evaluation and disaster forecasting to research the deformation rupture, instability mechanism, and failure mode of the rock roof in the mined-out areas.

The studies on the instability of the rock roof in the mining field have been a main topic both for scholars in China and abroad. For example, according to elastic thin plate theory, Wang et al. (2006) analyzed the fracture instability characteristics of the roof under different mining distances in the mining work face. Wang et al. (2008a) analyzed the rheological failure characteristics of the roof in the mined-out areas through combining the thin plate and rheology theories. Pan et al. (2013) had conducted the analytical analysis of the variation trend of the bending moment, the deflection, and the shear force of the hard roof in the mining field. This research is inclined to adopt traditional analytic methods to probe into the roof stability. New theories and methods have been used in recent years. Zhao et al. (2010) utilized the catastrophe theory to set up vertical deformation model of the overlapping roof in the mined-out areas, and put forward the criteria for evaluating the roof stability. Wang et al. (2013c) analyzed the chaos and stochastic resonance phenomenon produced in the roof during the evolutionary process of the rock beam deformation. Meanwhile, some numerical computation methods were applied in discussing the mechanical response of rock plate or beam. Wang et al. (2008a) analyzed the blast-induced stress wave propagation and the spalling damage in a rock plate by using the finite-difference code. Nomiko et al. (2002) researched the mechanical response of the multijointed roof beams using two dimensional distinct element code. Mazor et al. (2009) examined the arching mechanism of the blocky rock mass deformation after the underground tunnel being excavated using the discrete element method. Cravero and Iabichino (2004) discussed the flexural failure of a gneiss slab from a quarry face by virtue of linear elastic fracture mechanics (LEFM) and finite element method (FEM).

In summary, though many research achievements have been made, the most results still lack laboratory testing and need to be verified. In addition, some numerical calculations were conducted based on the continuum mechanics, which could not reflect the spatial heterogeneity and the anisotropic effect of the roof in the mining field. Only a few researchers utilized the discrete element methods to study the macromechanical

Advances in Rock-Support and Geotechnical Engineering
http://dx.doi.org/10.1016/B978-0-12-810552-8.00001-5

response of the rock plate, and did not further explore the microscopic damage of the rock plate. Therefore, a new loading device was developed to study the rock-arch instability characteristics of the plate, and particle flow code (PFC) was used to further probe into the microscopic damage of the rock plate under the concentrated and the uniform loading, respectively.

1.2 Loading Experiment of Rock Plate

1.2.1 Samples of Rock Plate

The rock samples used in the test were Hawkesbury sandstone, which obtained from Gosford Quarry in Sydney, Australia. The quartz sandstones which contained a small quantity of feldspars, siderite, and clay minerals were formed in marine sedimentary basin of the mid-Triassic, and located on the top of coal-bearing strata. The surface of specimen exhibited local red rather than white because of the content and distribution of iron oxide.

For the single-layer roof of the mined-out areas, it could be classified into two categories according to the thickness: the thin plate and the thick plate. And the roof was always made up of various combinations of the thin plates and the thick plates. Thus, according to the definition of the thin plate and the thick plate in elastic mechanics, the specimen size of the thick plate was deigned to 190 mm × 75 mm × 24 mm (length, width, and thickness) and that of the thin plate was deigned to 190 mm × 75 mm × 14 mm (length, width, and thickness). The specimens were obtained by cutting the same sandstone in the laboratory of School of Mining Engineering, University of New South Wales. The physical–mechanical parameters of rock plates were shown in Table 1.1.

1.2.2 Loading Equipment

The MTS-851 rock mechanics testing machine was selected as loading equipment, and the load was controlled by vertical displacement and loading rate was set 1×10^{-2} mm/s (Potyondy and Cundall, 2004). The vertical force and displacement occurred in the process of the test and were automatically recorded in real time by a data acquisition system.

As shown in Fig. 1.1, the concentrated and the uniform-loading test sets mainly consisted of three parts. The top was a point-loading for the concentrated loading or an assembly of the steel balls for the uniform loading. The middle was a loading framework which included four bolts with nuts connecting the steel plates on both sides, and the lateral pressure cell was placed between the deformable steel plate and the thick steel plate so as to monitor the horizontal force. The capacity of the lateral pressure cell Low Pressure X Type (LPX) was 1000 kg. The bottom was a rectangle steel foundation, the rotatable hinge supports were set on both sides of the loading framework to maintain connecting with the steel plates.

1.2.3 Acoustic Equipment and Data Acquisition System

To monitor the cracks initiated and identify the failure location of the rock plate, the USB Acoustic Emission (AE) Nodes were used in the test. The USB AE Node is a single channel AE digital signal processor with full AE hit and time based features. In the test there were four USB AE nodes being connected to a USB hub for multichannel operation (Fig. 1.2). All these AE nodes were made in MISTRAS Group, Inc., in the United States.

TABLE 1.1 Physical and Mechanical Parameters of Rock Plates

Name	Density (kg/m^3)	Elastic Modulus (GPa)	Poisson Ratio	Cohesion (MPa)	Friction Angle (Degrees)	Tensile Strength (MPa)	Compression Strength (MPa)
Sandstone	2650	2.7	0.20	2.8	45	0.95	13.5

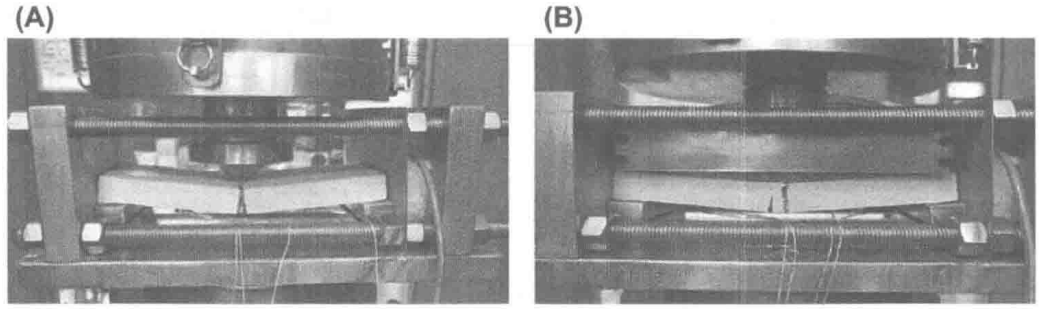

FIGURE 1.1 Loading experiment for the rock plate. (A) Concentrated loading. (B) Uniform loading.

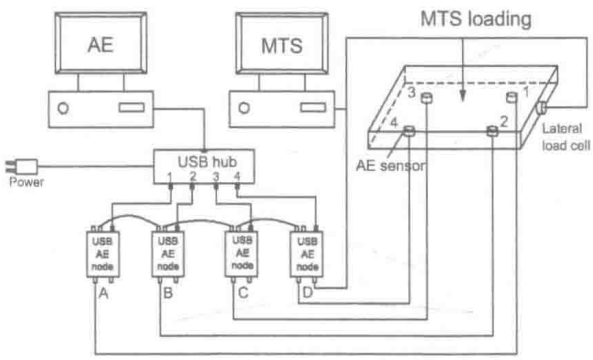

FIGURE 1.2 Mechanics Testing System (MTS) connection with acoustic emission monitoring system diagram.

1.3 Experiment Results and Analysis

1.3.1 Characteristic of Force–Displacement Curve

As shown in Fig. 1.3, the vertical force-displacement curves appeared two peaks under both the concentrate loading and the uniform loading, and the second peak value is higher than the first one. The thin rock plate showed the similarity cases in the test with the thick plate; only the peak values of the vertical and the horizontal force were lower than that of the thick one. In general, the curves of

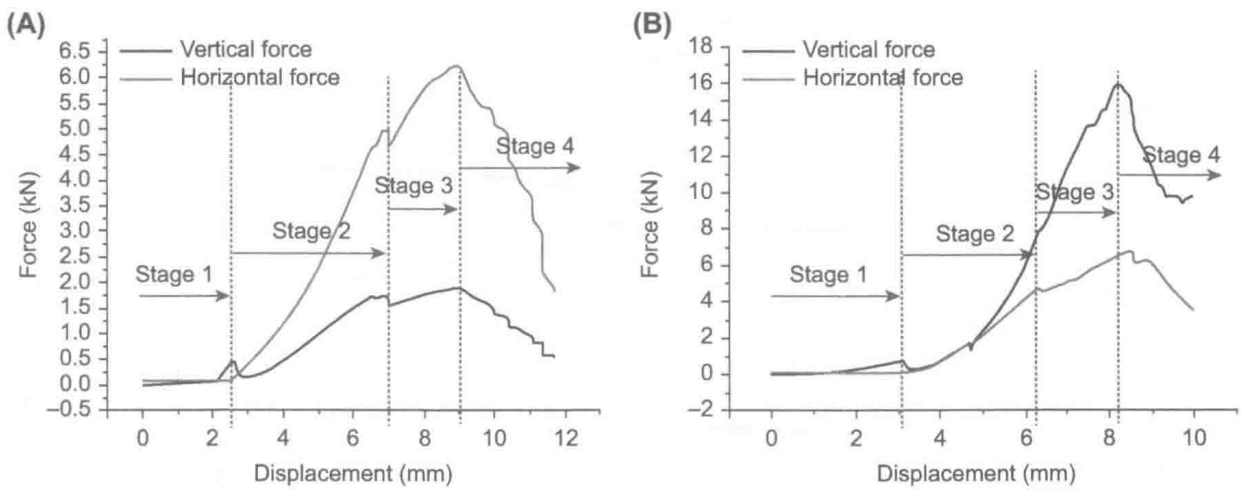

FIGURE 1.3 Force–displacement curves under different loading conditions. (A) Concentrated loading. (B) Uniform loading.

the force–displacement could be classified as four mechanical response stages as follows (Fig. 1.1A):

Stage 1: The rock plate was in the small deformation elastic stage. With the vertical force slowly increasing, the vertical displacement grew gradually. On the contrary, the horizontal force showed a slight decrease, which was mainly caused by the slight horizontal shrink of the rock plate during the loading process.
Stage 2: The rock plate produced a brittle rupture and formed the rock-arch structure. As the vertical displacement went to about 2.5 mm, the vertical force appeared to first increase abruptly and then drop sharply in a small interval, which indicated the rock plate producing a brittle rupture. Subsequently, the rock-arch structure was formed under the vertical and the horizontal reaction forces, and the horizontal force started to increase.
Stage 3: The rock-arch structure began to bear loads and produced deformation. With the vertical force increasing, the middle hinge point of the rock-arch structure moved down, and the two flanks of the rock-arch rotated around the hinge point, respectively. Such kinds of motion would stretch the rock-arch structure in the horizontal direction and squeezed the plate in two sides, and the horizontal force showed a significant growth.
Stage 4: The hinged rock-arch structure became unstable. With the vertical force continuously increasing, the middle hinged point of the rock-arch structure moved down constantly, and when the hinged point exceeded the horizontal line formed by the hinged point and two ends of the plate, the rock-arch structure became thoroughly unstable.

Under the uniform loading, the damage and fracture extent of the rock plate was more serious than that under the concentrated loading, especially at the two ends of the rock plate (Fig. 1.1B). As shown in Fig. 1.3, the load–displacement curve showed similarity with the concentrated loading, and the peak value of the vertical force was greater than that under the concentrated loading.

1.3.2 *Acoustic Characteristic of the Rock-Plate Failure*

As shown in Fig. 1.4, in the beginning of the stage two, the AE hits under the uniform loading were greater than that under the concentrated loading, which was about 5000 and 4500, respectively. In Stage 3 and Stage 4, the AE hits were also greater and more evenly distributed under the uniform loading compared with the concentrated loading, which was about 5000 and 3000, respectively.

As shown in the AE location map (Figs. 1.5 and 1.6), the results showed obvious differences in the initial crack position and the cracks distribution of the rock plate under different loading conditions. When the rock-arch structure went into instability, there also showed the differences in the damage extent and scope between the two loading methods. All in all, the results of AE hits and location showed the over-damage extent and scope of the rock plate caused by the uniform loading were more serious than that under the concentrated loading condition.

1.4 Numerical Simulations of the Loading Test

1.4.1 *Parameters Calibration of the Rock Plate*

The rock plate was treated as the porous and solid material that consisted of particles and cement bodies. The force–displacement curve was simulated under the concentrated loading using the three-dimensional particle flow code (PFC3D).

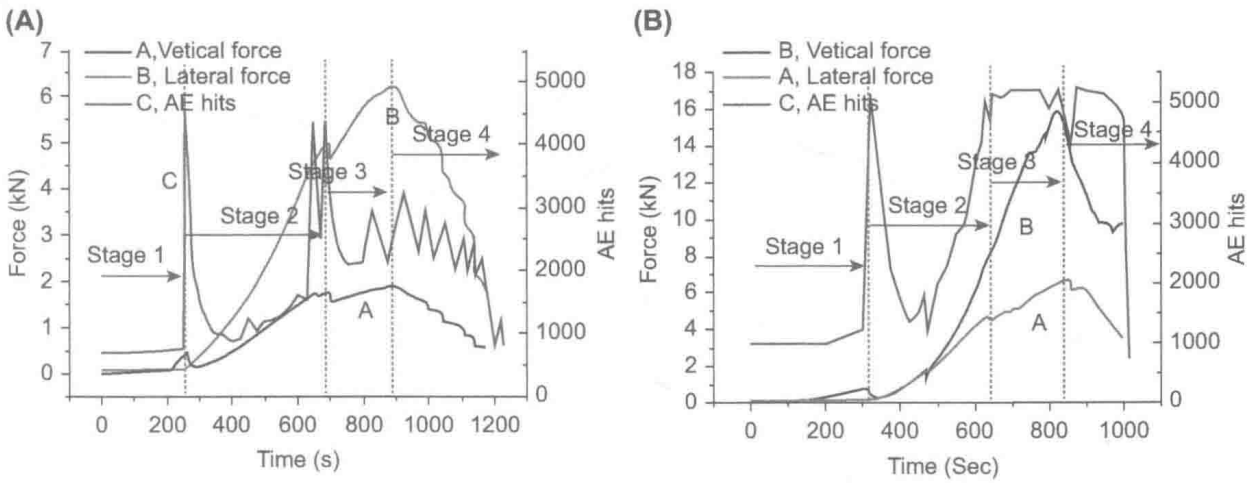

FIGURE 1.4 Acoustic emission hits and force–displacement curves under different loading conditions. (A) Concentrated loading. (B) Uniform loading.

Before the numerical simulation model could be built, the microparameters needed to be adjusted repeatedly and finalized until the macromechanical parameters calculated were consistent with the physical macromechanical parameters.

The microparameters required to be adjusted were as follows: ρ is ball density, R_{min} is minimum ball radius, R_{ratio} is ball size ratio, $\overline{\lambda}$ is parallel-bond radius multiplier, E_c is ball–ball contact modulus, $\overline{E}_c$ is parallel-bond modulus, k_n/k_s is ball stiffness ratio, $\overline{k}_n/\overline{k}_s$ is parallel-bond stiffness ratio, μ is ball friction coefficient, $\overline{\sigma}_c$ is parallel-bond normal strength, and $\overline{\tau}_c$ is parallel-bond shear strength. The microparameters required to be adjusted are listed in Table 1.2.

1.4.2 The Computational Model

Take the thick plate 190 mm × 75 mm × 24 mm (length, width, and thickness) as an example to show how to build the numerical calculation model.

First, a parallelepiped specimen consisting of arbitrary particles confined by six frictionless walls was generated by the radius expansion method. Second, the radii of all particles were changed uniformly to achieve a specified isotropic stress so as to reduce the magnitude of locked-in stresses that would develop after the subsequent bond installation. In this paper the isotropic stress was set to 0.1 MPa. Third, the floating particles that had less than three contacts were eliminated. Fourth, the parallel bonds were installed throughout the assembly between all particles that were in near proximity to finalize the specimen. Finally, the loading devices were installed on the rock plate as shown in Fig. 1.7.

A square wall with sides 10 mm was made on the top of the rock plate as the concentrated loading, and the loading rate was set to 0.01 m/s (The loading rate could be regarded as the quasistatic loading). The two cylinder walls were placed on the right and left at the bottom respectively as supporting base. The two walls located on both sides could install the initial horizontal force at the specified value. During the loading, the cracks generated in the rock plate were monitored in real time. The red cracks represented the tensile fracture, and the black ones represented the shear fracture.

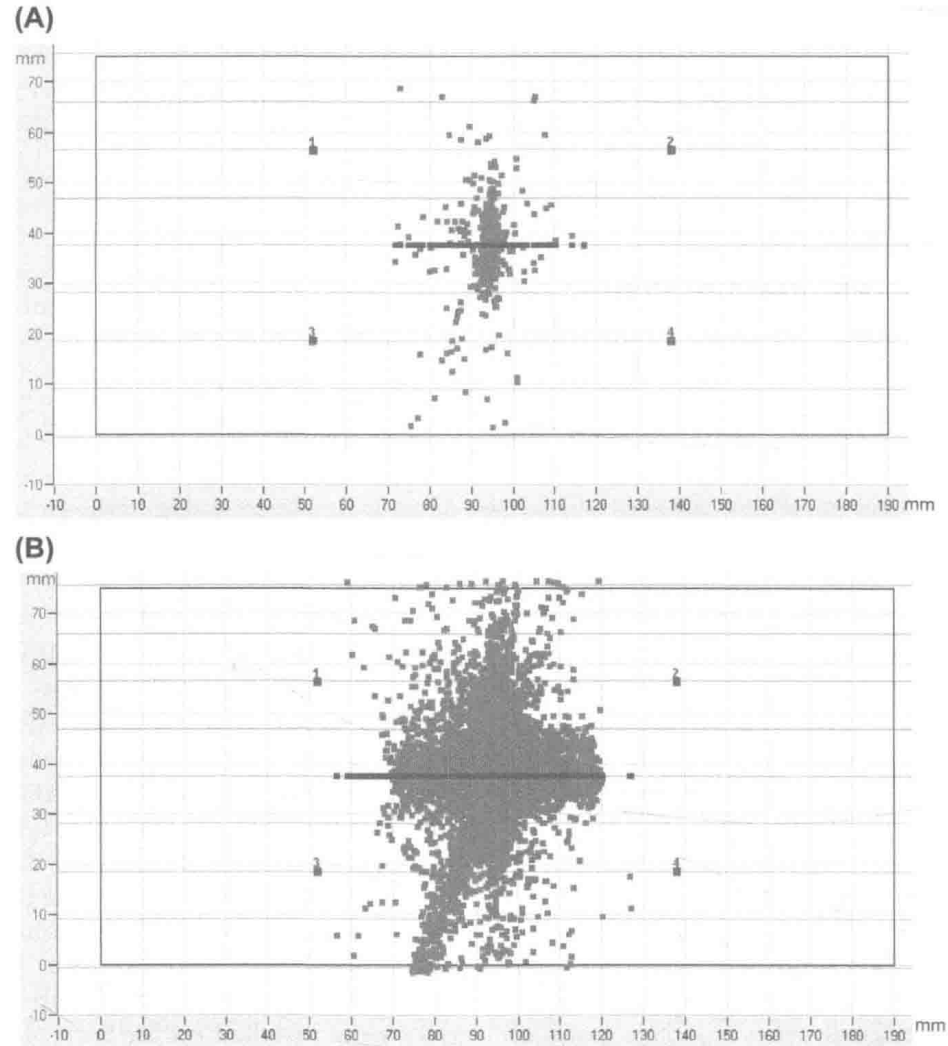

FIGURE 1.5 Acoustic emission location of rock plate under concentrated loading. (A) Initial cracks. (B) Ultimate cracks.

1.4.3 Analysis of Numerical Simulation Results

As shown in Fig. 1.8, since the interaction forces among the particles were simplified in PFC3D, there were some differences in the vertical force–horizontal force–displacement simulated curves compared with the physical experimental results, but the variation trend of the curves was basically the same for two cases, so the physical experimental results confirmed the numerical credibility.

In the elastic deformation stage (Fig. 1.9A), the displacement vector field described that a slight elastic deformation produced in the rock plate, and at the same time there was no crack generated in this stage. In the brittle rupture

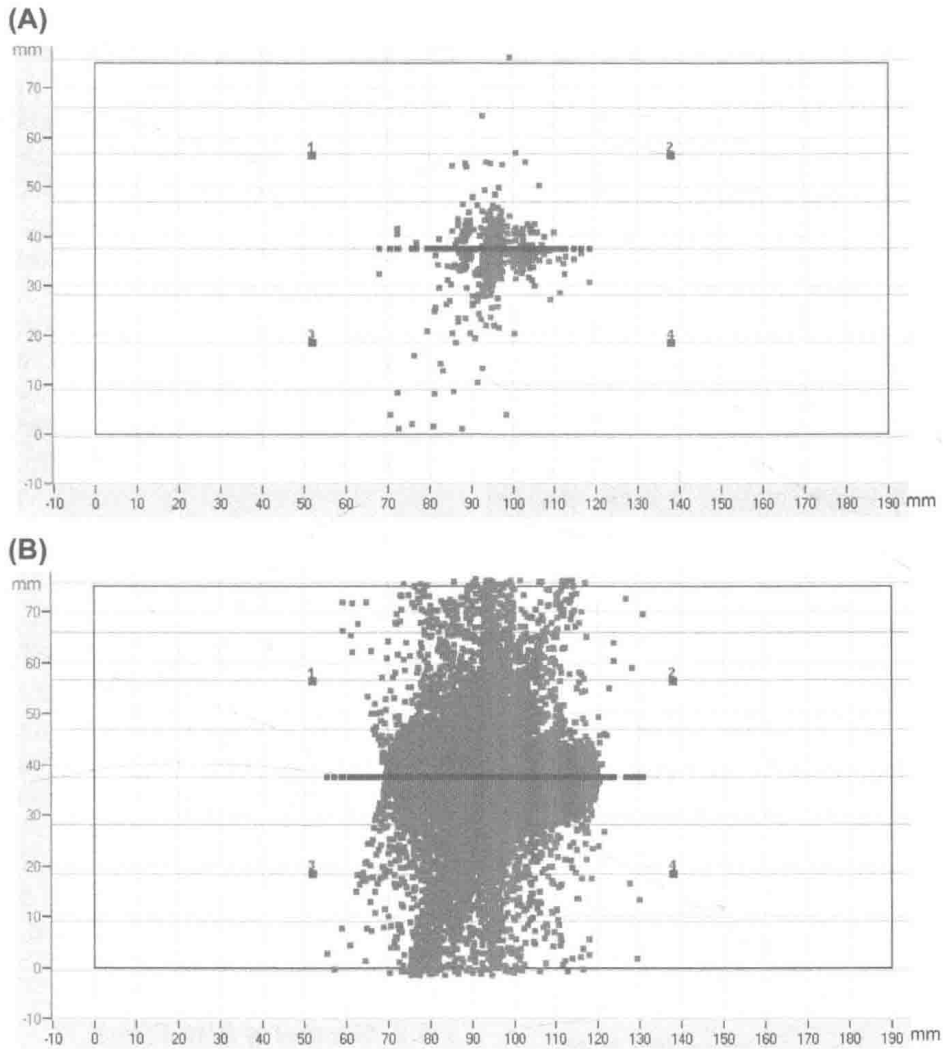

FIGURE 1.6 Acoustic emission location of rock plate under uniform loading. (A) Initial cracks. (B) Ultimate cracks.

TABLE 1.2 Microparameters of the Model in PFC3D

ρ (kg/m^3)	R_{min} (mm)	R_{ratio}	μ	$\overline{\lambda}$	E_c (GPa)	$\overline{E}_c$ (GPa)	k_n/k_s	$\overline{k}_n/\overline{k}_s$	$\overline{\sigma}_c$ (MPa)	$\overline{\tau}_c$ (MPa)
2650	1.2	1.66	0.5	1.0	2.7	2.8	1.8	1.8	16	16

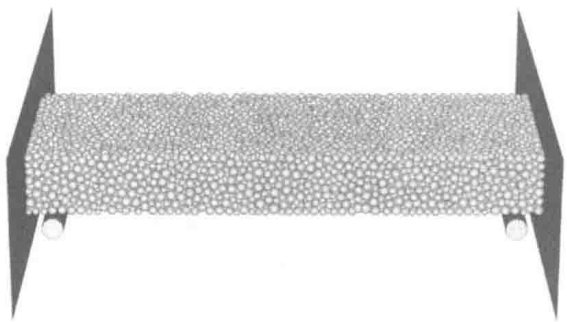

FIGURE 1.7 Computational model and its boundaries.

stage (Fig. 1.9B), there was many tensile cracks produced in the rock plate, and these tensile cracks formed a tensile failure plane in the rock plate. In the rock-arch bearing load stage (Fig. 1.9C), the shearing and tension cracks emerged in the hinged plane and both ends of the rock plate. In the rock-arch instability stage (Fig. 1.9D), the rock-arch structure had a large deformation, and parts of the particles in the hinged plane of both sides had escaped from the rock plate mainly due to the squeezing fracture.

As shown in Fig. 1.10, the number of shear cracks obeyed the S-figure curve during the whole mechanical response process, which was also applicable to the tensile cracks only after the brittle rupture. When the vertical displacement reached around 1.0 mm, the number of the tensile cracks surged to 300. As the displacement varied in the interval 1.0–2.5 mm, the crack development kept almost unchanged. However, with the displacement continuously increasing, the number of both shearing and tension cracks kept increasing, the hinged planes and both ends of the rock plate showed the mixture of shearing and tensile cracks. As rock-arch structure went into instability, the number of cracks still kept significant increasing until the displacement reached to 6 mm.

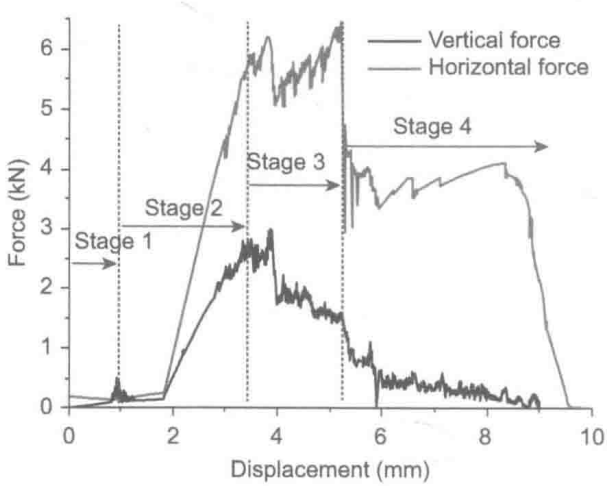

FIGURE 1.8 Force–displacement relationship curves.

1.5 Factors Sensitive Analysis of Rock-Arch Instability

1.5.1 Material Parameter Effect

As shown in Fig. 1.11, with the friction coefficient of the particles increasing, the peak values of the vertical force and the horizontal force of the rock-arch structure also increased. This was mainly because the friction growth enhanced the peak strength of the rock material, namely after breakage of the parallel bond, the strength of the rock material often contributed to the contact friction of the particles.

1.5.2 Geometry Size Effect

As shown in Fig. 1.12, the length, width, and thickness of the rock plate changed, respectively, to reveal the size effect on the instability of the rock-arch structure. With the length of the rock plate increasing, the peak values of the vertical and the horizontal force were gradually decreased, and the whole variation interval was small. With the width and the thickness of the rock plate increasing, the peak values of the vertical and the horizontal force showed obvious growth. In short, the response of the rock-arch structure instability was more sensitive to the width and thickness compared with the length.